African Journal of Pharmaceutical Research and Development
Available online at https://ajopred.com
Vol. 15 No.3; pp. 63-76 (2023)

Original Research Article

IN SILICO IDENTIFICATION OF THE ANTHRAQUINONE PIGMENT MORINDONE AS A *PLASMODIUM FALCIPARUM* LACTATE DEHYDROGENASE (*PF*LDH) INHIBITORY ANTIMALARIAL DRUG LEAD

OLUSEGUN SAMSON AJALA[1,*], OLAYINKA HANNAH DADA[1], DOLAPO OMOLADE INNOCENT-UGWU[1], PEACE UDODIRI OKECHUKWU[1]

1. Department of Pharmaceutical Chemistry, Faculty of Pharmacy, University of Lagos, CMUL Campus Idiaraba, P.M.B. 12003, Surulere, Lagos

ABSTRACT

Plasmodium falciparum Lactate Dehydrogenase (*Pf*LDH) inhibition could be exploited for the purpose of fast parasitemia clearance necessary for the treatment and/or prevention of cerebral malaria (CM). This investigation was aimed at *in silico* evaluations of *Morinda lucida*-based anthraquinones for their potential *Pf*LDH inhibitory activities via interference with the enzyme's cofactor (NADH) redox function. Thirty-seven (37) anthraquinones of *Morinda lucida* were docked to the NADH-binding site of a ternary model of *Pf*LDH. Considering -8.0 Kcal/mol binding affinity as comparable to the -10 Kcal/mol binding affinity of NADH, top nine of the docked ligands (binding energies -8.3Kcal/mol to -9.7 Kcal/mol) were initially selected as hits and subjected to drug-likeness screening using the five (Lipinski, Ghose, Verber, Egan and Muege) drug-likeness filters of the SwissADME webserver. Six of them, showing no violation of any of the stipulations of each of the five filters were subjected to toxicity profiling predictions with Protox II webserver, leading to the selection of morindone (Binding energy -8.4 Kcal/mol; predicted LD_{50} 7000 mg/Kg) as the safest. Subsequent Molecular Dynamics (MD) simulations on morindone-*Pf*LDH complex showed that both morindone and its *Pf*LDH complex were stable over a 50 ns simulation, the RMSD-time plot of the complex showing a convergence of its initial and instantaneous structures at around 5 ns with deviations largely around 3 Å throughout the 50 ns simulation period. The *Morinda lucida*-based anthraquinone pigment morindone is hereby uncovered as a potential lead or template for the discovery of *Pf*LDH inhibitory antimalarials deployable for the treatment of severe falciparum malaria and its cerebral malaria prognosis.

ARTICLE INFO

Received 16 October, 2023
Revised 14 December, 2023
Accepted 20 December, 2023

KEYWORDS

Anthraquinones,
Falciparum malaria,
Lactate dehydrogenase,
Morinda lucida,
Plasmodium falciparum

INTRODUCTION

Malaria is a parasitic disease transmitted by the bite of female anopheles mosquito in which *Plasmodium spp.* causative parasites complete their life cycle [1, 2]. Five *Plasmodium spp* are known to cause infection in man [2[but only one (*P. falciparum)* is responsible for more than 99% of the severe or deadly form of the disease, manifesting mostly as CNS complications collectively referred to as cerebral malaria (CM) [3]. Given that the pathophysiology of CM is the prolonged microvasculature exposure to the blood stages of the parasite [4], fast parasitaemia clearance is a critical goal in *falciparum* malaria treatment if its rising CM prognosis and devastating

***Corresponding author:** olajala@unilag.edu.ng; +234-803 562 2151

https://doi.org/10.59493/ajopred/2023.3.8 ISSN: 0794-800X (print); 1596-2431 (online)

effects on both children and adult populaces in the sub-Saharan Africa must be curtailed [5-8].

Identification of *falciparum* targets druggable for the sole aim of fast parasitaemia clearance and the computer-assisted identification of potential interactives of such targets could be a giant stride in the direction of discovery of new antimalarial agents with potentials of treating and/or preventing CM and other complications of severe malaria [9]. A highly promising example of such targets is the enzyme *Plasmodium* Lactate dehydrogenase (*P*LDH), the inhibition of which has great propensities for highly selective fast blood shizonts clearance as narrated below.

Plasmodium *spp*. encode their blood stages (both asexual and sexual) anaerobic because their mitochondria are encoded for anabolic (or biosynthetic) reasons and not in any way for the primary oxidative phosphorylating ATP-synthesizing tricarboxylic acid or Kreb's cycle [10]. In fact, enzymes of the Kreb's cycle have been demonstrated to be lacking in the blood stages of *Plasmodium spp* [10,11]. The energy metabolism implication of this phenomenon is that these stages of the organism's life cycle would have to depend absolutely on glycolysis, making them highly susceptible to glycolysis inhibition. One glycolytic pathway enzyme strategically positioned to achieve this purpose is Lactate dehydrogenase, the last enzyme of the pathway catalysing the conversion of pyruvate to lactate with the production of two ATP molecules [12]. Inhibiting *Plasmodium falciparum* Lactate Dehydrogenase (*Pf*LDH) could therefore be a malaria chemotherapeutic strategy with considerably fast blood schizonts (parasitaemia) clearance and hence, CM prognosis - prohibiting. Moreover, it is worthy of note that LDH is activated only in low oxygen tensions or in mitochondrial/mitochondrial tricarboxylic acid pathway enzymes deficiencies, as is the case with the blood schizonts of *Plasmodium spp* [13,14]. Inhibiting Plasmodial LDH is therefore expected to be largely safe as most of the host cells would depend on the rather efficient tricarborxylic acid cycle for their energy production, the few ones that could be momentarily anaerobic in low oxygen beds also being potentially less susceptible as the human LDH isozyme differs considerably at the NADH binding region of its active site [15,16,17].

As is the case with most cofactor-dependent enzymes, *Pf*LDH inhibition at the substrate binding site is NADH binding-directed, creating a possibility of non-competitive active-site-inhibition [18]. However, a more easily visualised non-competitive inhibition is interference with NADH's redox roles in the catalysis [19] which could be achieved either sterically by structural mimicry or electronically by interference with its redox activities. While structural mimicry would necessitate the use of huge flexible molecules which mostly would be non-drug-like, redox intrusion could be carried out by compounds of diverse structures and sizes endowed with redox capabilities. One group of naturally occurring redox-active compounds that could be explored for this purpose are the anthraquinones [20,21].

Anthraquinones are essentially 9, 10-dioxoanthracenes, though a few 1, 4-dioxo isomers do exist [22]. They constitute the most diverse of the quinones chemical space, benzoquinones and naphthoquinones being the other two major subgroups of the super family [22]. Anthraquinones are widely distributed in nature, occurring in bacteria, fungi, animals and plants. They are broadly classified, on biosynthetic accounts, into polyketide and shikimate anthraquinones [23]. The shikimate anthraquinones, e.g., morindone, alizarin and rubiadin, are also often referred to as Rubia anthraquinones. They are characterized by having substitution only on ring C (Fig. 1), a product of the isoprenoid pathway that is in clear distinction from the shikimate pawthway from which rings A and B originate [24,25]. The Polyketide anthraquinones, e.g., emodin, chrysophanol and physicion, characterised by substitution on both rings A and C, and especially by the existence of hydroxyls at C-1 and C-8 (Fig. 1), are derived from one acetyl CoA unit extended by seven malonyl CoA units via an octakitide chain [26,27]. They are commonly found in fungi, lichens and the Rhamnaceae, Polygonaceae and leguminoceae plant families.

Morinda lucida is a Rubiaceae species that has been used, *inter alia* for the treatment of malaria in tropical traditional medicine, its phytochemical exploration over the years showing it to be richly endowed with a diversity of secondary metabolites of which anthraquinones are key. In fact, anthraquinones and derivatives are the prime suspects of the plant's main pharmacological properties including its antimalarial activities [28].

In the light of the above, we, in the current investigation, hypothesized the antimalarial properties of *M. lucida* as, at least, in parts, due to its anthraquinone contents. Furthermore, the *Pf*LDH inhibitory action mechanism of this activity via interference with the coenzyme NADH function was conjectured. In a bid to explore the veracity of these conjectures, we docked thirty-seven (37) anthraquinones of *M. lucida* to the NADH binding site of the enzyme to generate potential hits which were further subjected to webserver-based Pharmacokinetics/drug-likeness and toxicity profilings to arrive at a potential lead, morindone, the *in vivo* binding-stability possibility of which was further evaluated by molecular dynamics simulation studies.

MATERIALS AND METHODS

Materials and Software

An HP ProBook equipped with intel Core i5, 500GB Hard Disk, 8 GB RAM and WiFi was the main hardware; Protein preparations were done using UCSF Chimera 1.14 [29]; 2D and 3D anthraquinone-*Pf*LDH interactions at the NADH binding site were simulated using BIOVIA Discovery studio visualizer 2021 [30]; multiple ligands docking was carried out with PyRx molecular docking software equipped with AutoDock Vina and Open Babel plugins [31]; SwissADME [32] and Protox II [33] webservers were used for pharmacokinetics and toxicity profilings respectively; molecular dynamics simulations were performed using the University of Arkansas for Medical Sciences (UAMS) simlab WebGro webserver (34); other helpful webservers in the course of this study include: RCSB Protein

Databank (PDB) [35], Pubchem [36], PRODRG [37], CASTp [38] and Uniprot [39].

Protein Preparation

An X-ray crystal model of a ternary *Pf*LDH co-complexed with NADH (PDBID 1T2C; Resolution 2.01 Å), was uploaded into Chimera 1.14 workspace by direct fetch. All non-standard residues including the co-crystalized inhibitor, the coenzyme NADH and water molecules were removed. Hydrogen atoms and amber charges were added and the structure subsequently minimized using 200 steepest descent and 10 conjugate gradient steps of the energy minimization algorithm of the software [40]. The ensuing prepared protein structure was saved for subsequent uses.

Anthraquinone Ligands Preparation

Thirty-seven (37) anthraquinones of *Morinda lucida* [41, 42] were retrieved from the Pubchem database as structure data files and built into a one-file library of anthraquinones. The library file was uploaded into the Open Babel workspace of PyRx for energy minimization and subsequent conversion into pdbqt (or autodock-compliant) ligands.

Multiple Ligands Docking

The prepared *Pf*LDH protein was uploaded into the PyRx docking workspace and made macromolecule. The anthraquinone library file was imported into the docking workspace and the 37 anthraquinones therein selected as ligands before the autodock vina algorithm was run, using the three-dimensional coordinates of NADH binding site as guide for the auto-generated docking gridbox with the following coordinates (in Angstroms): center_x = 32.6885538462; center_y = 16.5121670712; center_z = 11.2329541721; size_x = 21.8024935635; size_y = 19.3277442171; size_z = 20.9429268838.

Estimation of Inhibition Constant Ki

Inhibition constant Ki of each of the initial nine anthraquinone hits was determined using the following relationship:

$Ki_{pred} = \text{exponential}^{(\Delta G/RT)}$,

where Ki_{pred} is the predicted inhibition constant, ΔG is the binding free energy (docking score) (kcal/mol), R is the gas constant (1.98 $calK^{-1}$ mol^{-1}), and T is the room temperature in Kelvin (298.15 K) [43].

Docking Protocol Validation

To validate the above-described docking protocol, NADH structure data file was included in the the anthraquinone library file and docked alongside the anthraquinones. The coordinates of the lowest-energy pose of the docked NADH molecule was superimposed on those of its co-crystalized counterpart, using the BIOVIA Discovery Studio to visualize and calculate deviations as Root Mean Square Deviation (RMSD).

Drug-likeness and Toxicity Profilings

Top nine anthraquinones from the docking experiment were screened with the five (i.e., Lipinsky, Verber, Ghose, Muegge and Egan) drug-likeness filters of the SwissADME webserver. Canonical SMILES [44] of the anthraquinone ligands were the main inputs while a rather strict condition of not failing any of the stipulations of each filter was set for drug-like anthraquinones selection. The potential carcinogenicities, organ toxicities and LD_{50} of selected compounds were subsequently evaluated using Prtox II webserver.

Molecular Dynamics Simulations

The stability of the complex of *Pf*LDH with the safest of the drug-like anthraquinone ligands (morindone) was explored with molecular dynamics simulations using Webgro, the University of Arkansas for Medical Sciences (UAMS) webserver for molecular dynamics simulation. Independent variable parameters were set as follows: Box type was triclinic with SPC water model; GROMOS9643a1 was selected as force field; equilibrium temperature was 300 K, while simulation time was set at 50 ns. Morindone-*Pf*LDH complex was prepared as a pdb file with BIOVIA Discovery Studio; Morindone topology file was prepared with PRODRG webserver, using moridone's coordinates extracted from its *Pf*LDH complex text format.

RESULTS

Multiple Ligand Docking

The docked thirty-seven anthraquiniones demonstrated binding affinities ranging from -6.6 Kcal/mol to -9.7 Kcal/mol. (Table 1).

Initial Hits Selection

Hits selection based on the preset ≤ 8.0 Kcal/mol minimum binding affinity afforded the top nine of the 37 docked ligands arranged in order of binding affinity. Estimated inhibition constant (Ki) for NADH was 69 nM while those of the nine hits ranged between 103 nM and 421 nM, showing better relativities in their *Pf*LDH-binding interactions, compared to mere docking scores (Table 2). It is worthy of note that the first three of the aforementioned nine compounds are glycosylated anthraquinones (Fig. 2) while the later six are plain counterparts (Fig. 3).

Docking Validation

The coordinates of the co-crystalized NADH and those of its most stable docked conformation superimposed well with an RMSD of 1.82 Å (Fig. 4).

Drug-Likeness Screening

The first three of the nine anthraquinone hits showed varying degrees of violation of each of the SwissADME's five drug-likeness filters while each of the latter six showed no violation at all (Table 3). Moreover, while each of these six showed a bioavailability score of 0.55, the first three that showed various degrees of violations of the drug-likeness filters showed a bioavailability score of 0.17 each (Table 3).

Toxicity Profiling

The six drug-like anthraquinone hits profiled for toxicity gave at least 5000 mg/Kg LD_{50} value with no hepato- or any other organ toxicity activity. Toxicity end point measurements showed them to be neither cytotoxic nor carcinogenic. They all however showed potential mutagenicity (Table 4).

Table 1: NADH and thirty-seven anthraquinones of *M. lucida* arranged in increasing order of *Pf*LDH-binding affinity (Kcal/mol)

S/N	Ligand	Binding Affinity (Kcal/mol)
1	NADH	-10.1
2	Morindin	-9.7
3	Lucidin-3-O-primveroside	-9.3
4	1,3,6-Trihydroxy-2-methylanthraquinone3-O-(6'-O-acetyl)-a-L-rhamnosyl-(1-2)-beta-D-glucoside	-8.9
5	2-acetyl-1-hydroxyanthraquinone	-8.4
6	Morindone	-8.4
7	morindone-5-methylether	-8.4
8	1,5-Dihydroxy-2-methoxy-6-methylanthraquinone	-8.3
9	1,6-dihydroxy-2-hydroxymethyl-5-methoxy-9,10-anthracenedione	-8.3
10	2-Formyl-1-hydroxyanthraquinone	-8.3
11	Copareolatin-6-methylester	-7.9
12	Soranjidiol	-7.9
13	1-Hydroxy-2-methylanthraquinone	-7.8
14	Munjistin methyl ester	-7.8
15	Munjistin	-7.8
16	2-Formylanthraquinone	-7.8
17	Chrysophanol	-7.8
18	Damnacanthol	-7.7
19	1-Methoxy-2-methylanthracene-9,10-dione	-7.7
20	6-hydroxyrubaidin	-7.7
21	rubiadin 1-methyl ether	-7.7
22	1,5,15-Tri-O-methyl morindol	-7.7
23	Lucidin	-7.6
24	Rubiadin	-7.6
25	damnacanthal	-7.6
26	1,2-Dimethoxyanthracene-9,10-dione	-7.6
27	Tectoquinone	-7.6
28	Alizarin 1-methylether	-7.6
29	3-Hydroxy-9,10-dioxo-anthracene-2-carbaldehyde	-7.5
30	nordamnacanthal	-7.5
31	9-oxoxanthenecarboxylic acid	-7.5
32	3-hydroxy-2-hydroxymethyl anthraquinone	-7.5
33	1,5,6-Trimethoxy-2-methyl-3-hydroxy-9,10-anthraquinone	-7.4
34	Questinol	-7.4
35	Digitolutein	-7.4
36	Subspinosin	-7.1
37	fraxidin	-6.6
38	4-Hydroxyanthraquinone-2-carboxylic acid	-6.6

Table 2: Binding affinities (Kcal/mol) and Inhibition constant Ki of NADH and top nine of thirty-seven anthraquinones of *M. lucida* docked to PfLDH. in decreasing order of binding affinity

S/N	Name	Binding Affinity (Kcal/mol)	Inhibition Constant(Ki)(nM)
1	NADH	-10.1	69
2	Morindin	-9.7	103
3	L3P	-9.3	155
4	TMG	-8.9	231
5	AHA	-8.4	381
6	Morindone	-8.4	381
7	MME	-8.4	381
8	DHMM	-8.3	421
9	DHMA	-8.3	421
10	FHA	-8.3	421

NADH = Nicotinamide Adenine Dinucleotide
L3P = Lucidin-3-primveroside
TMG =1,3,6-Trihydroxy-2-methylanthraquinone3-O-(6'-O-acetyl)-a-L-rhamnosyl-(1-2)- beta-D-glucoside
AHA = 2-acetyl-1-hydroxyanthraquinone
MME = Morindone-5-methyl ether
DHMM = 1,5-Dihydroxy-2-methoxy-6-methylanthraquinone
DHMA = 1,6-dihydroxy-2-hydroxymethyl-5-methoxy-9,10-anthracenedione
FHA = 2-Formyl-1-hydroxyanthraquinone

Table 3: Drug-likeness filter violations and bioavailability scores for top ten high-affinity anthraquinones

S/N	Compound	Lipinski	Ghose	Veber	Egan	Muegge	Bio. Score
1	Morindin	3	2	1	1	3	0.17
2	L3P	3	2	1	1	4	0.17
3	TMG	3	4	1	1	4	0.17
4	AHA	0	0	0	0	0	0.55
5	Morindone	0	0	0	0	0	0.55
6	MME	0	0	0	0	0	0.55
7	DHMA	0	0	0	0	0	0.55
8	DHMM	0	0	0	0	0	0.55
9	FHA	0	0	0	0	0	0.55

L3P = Lucidin-3-primveroside
TMG =1,3,6-Trihydroxy-2-methylanthraquinone3-O-(6'-O-acetyl)-a-L-rhamnosyl-(1-2)-beta-D-glucoside
AHA = 2-acetyl-1-hydroxyanthraquinone
MME = Morindone-5-methyl ether
DHMM = 1,5-Dihydroxy-2-methoxy-6-methylanthraquinone
DHMA = 1,6-dihydroxy-2-hydroxymethyl-5-methoxy-9,10-anthracenedione
FHA = 2-Formyl-1-hydroxyanthraquinone

Table 4: Organ toxicity and toxicity end point evaluations of six high-docking-score *Pf*LDH-binding anthraquinones with good drug-likeness properties

S/N	Compound	Predicted LD50 (mg/Kg)	Toxicity endpoints			
			Hepatotoxicity	Cytotoxicity	Carcinogenicity	Mutagenicity
1	AHA	5000	Not active	Not active	Not active	Active
2	Morindone	7000	Not active	Not active	Not active	Active
3	MME	5000	Not active	Not active	Not active	Active
4	DHMM	5000	Not active	Not active	Not active	Active
5	DHMA	5000	Not active	Not active	Active	Active
6	FHA	5000	Not active	Not active	Not active	Active

AHA = 2-acetyl-1-hydroxyanthraquinone
MME = Morindone-5-methyl ether
DHMM = 1,5-Dihydroxy-2-methoxy-6-methylanthraquinone
DHMA = 1,6-dihydroxy-2-hydroxymethyl-5-methoxy-9,10-anthracenedione
FHA = 2-Formyl-1-hydroxyanthraquinone

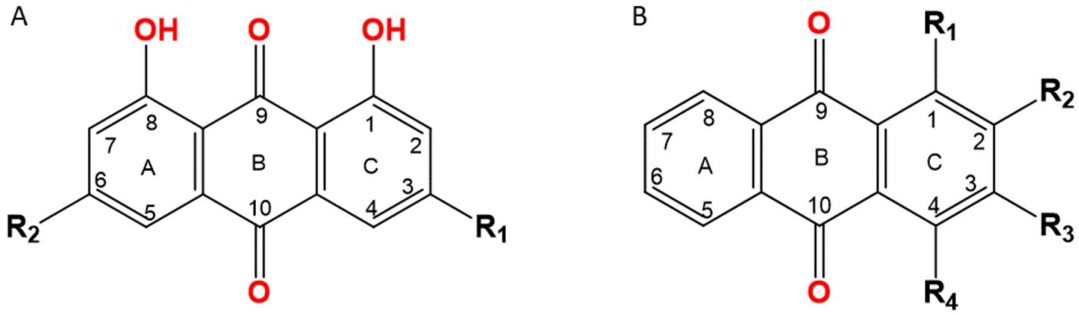

Fig. 1: A- general structure of the polyketide anthraquinones showing their characteristic substitutions on rings A and C. (R1, R2 could be hydrogen, hydroxyl, methyl or hydroxymethyl groups); B- general structure of the shikimate (or rubia) anthraquinones showing their characteristic only-ring-C substitutions. (While R1 is almost always hydroxyl/methoxy, R2, R3 and R4 range between hydrogen, hydroxyl, hydroxymethyl, and aldehydic groups)

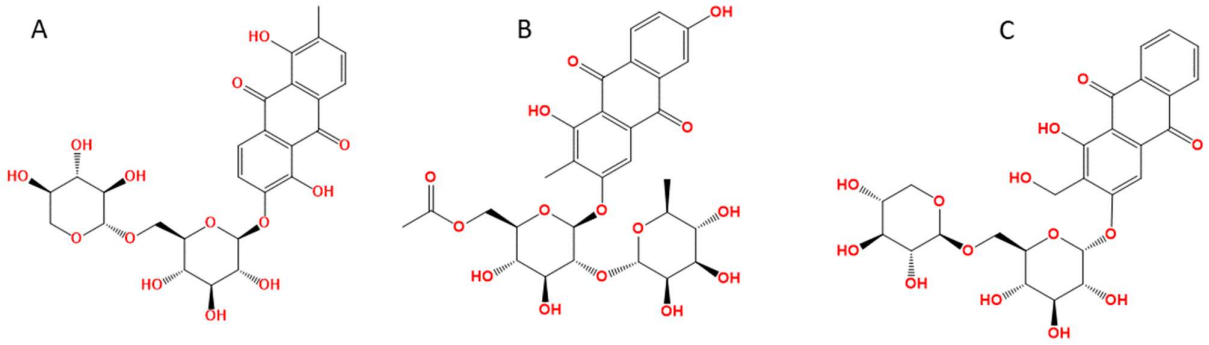

Fig. 2: Glycosylated anthraquuinones (A: morindin; B: Lucidin-3-primveroside and C:1,3,6-Trihydroxy-2-methylanthraquinone3-O-(6'-O-acetyl)-a-L-rhamnosyl-(1-2)-beta-D-glucoside, showing the highest *Pf*LDH-binding affinities of – 9.7, -9.3 and -8.9 Kcal/mol respectively, but violating the stipulations of Lipinski, Ghose, Verber, Egan and Muege drug-likeness filters to varying degrees.

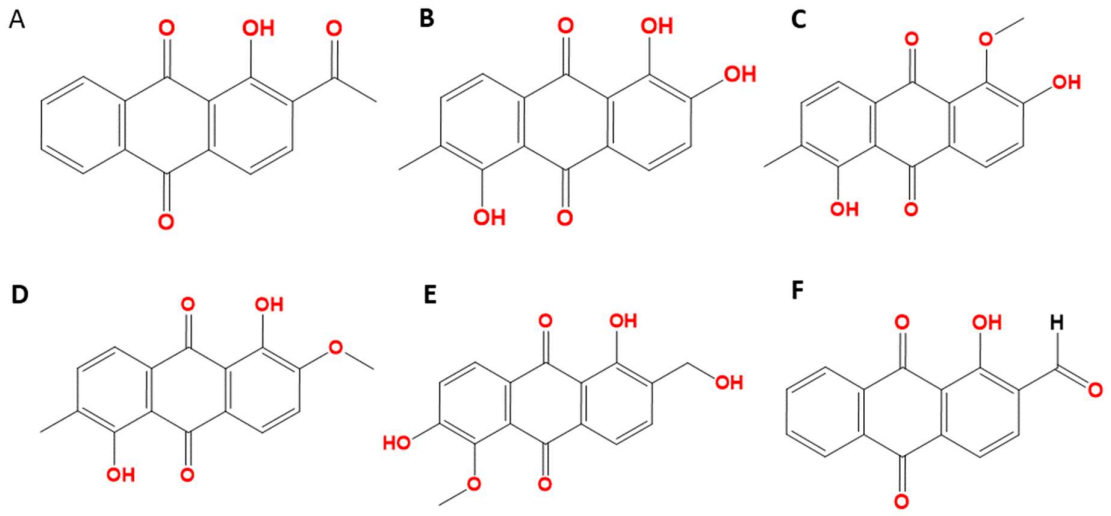

Fig. 3: Plain anthraquinones (A: 2-acetyl-1-hydroxyanthraquinone; B:morindone; C: morindone-5-methyl ether; D:1,5-dihydroxy-2-methoxy-6-methylanthraquinone; E:1,6-dihydroxy-2-hydroxymethyl-5-methoxy-9,10-anthracenedione; F:2-Formyl-1-hydroxyanthraquinone) with *Pf*LDH-binding affinities ≤ -8.0 Kcal/mol and violating none of the stipulations of any of Lipinski, Ghose, Verba, Egan and Muege drug-likeness filters.

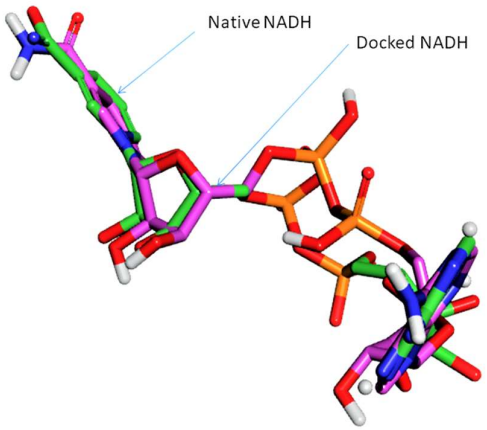

Fig. 4: Superimposed native (green colour) and docked (purple colour) NADH molecules (RMSD 1.82 Å)

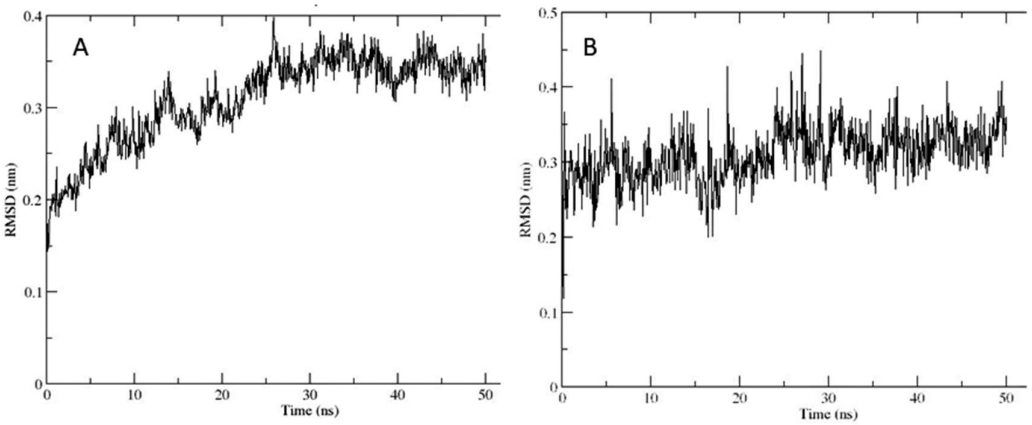

Fig. 5: A: RMSD of morindone-*Pf*LDH complex and B: RMSD of morindone at the binding pocket over a 50 ns simulation time.

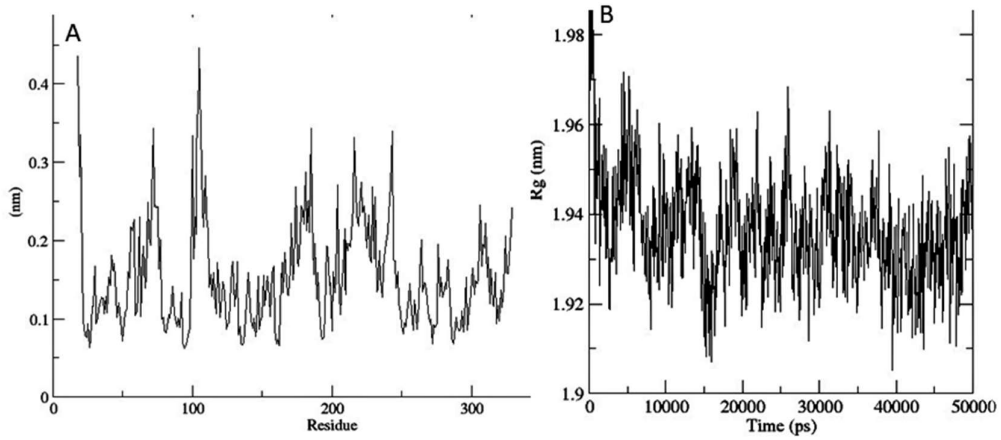

Fig. 6: A: RMSF and B: Radius of gyration of morindone-*PF*LDH complex over a 50 ns simulation time

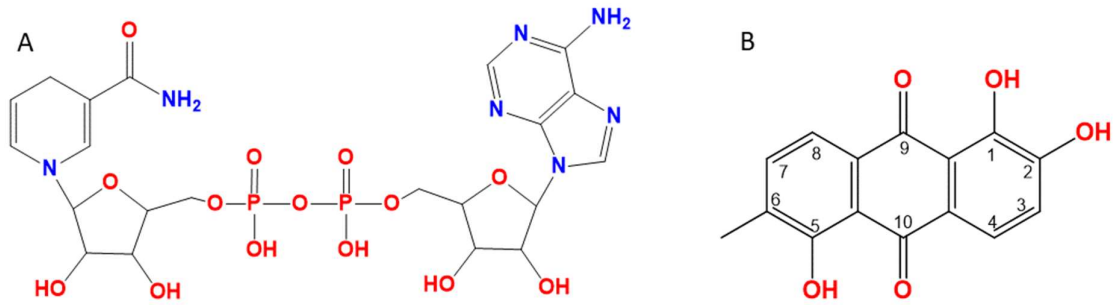

Fig. 7: 2D structures of A: NADH and B: morindone

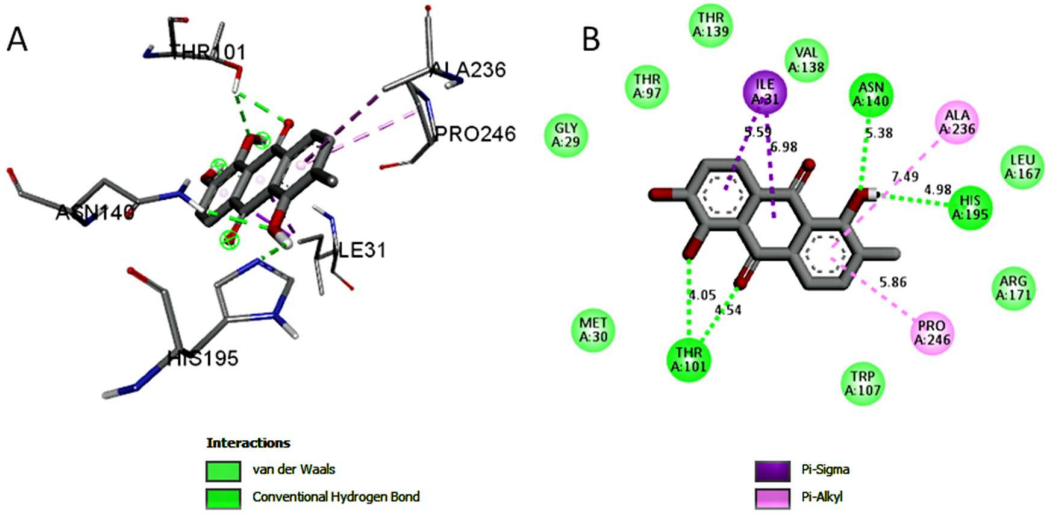

Fig. 8: A: 3D and B: 2D simulations of morindone interactions at the NADH binding site, showing conventional hydrogen bonding with THR 101 and ARG171; Pi-alkyl interactions with ALA236 and PRO 246, and a number of Van der Waals interactions.

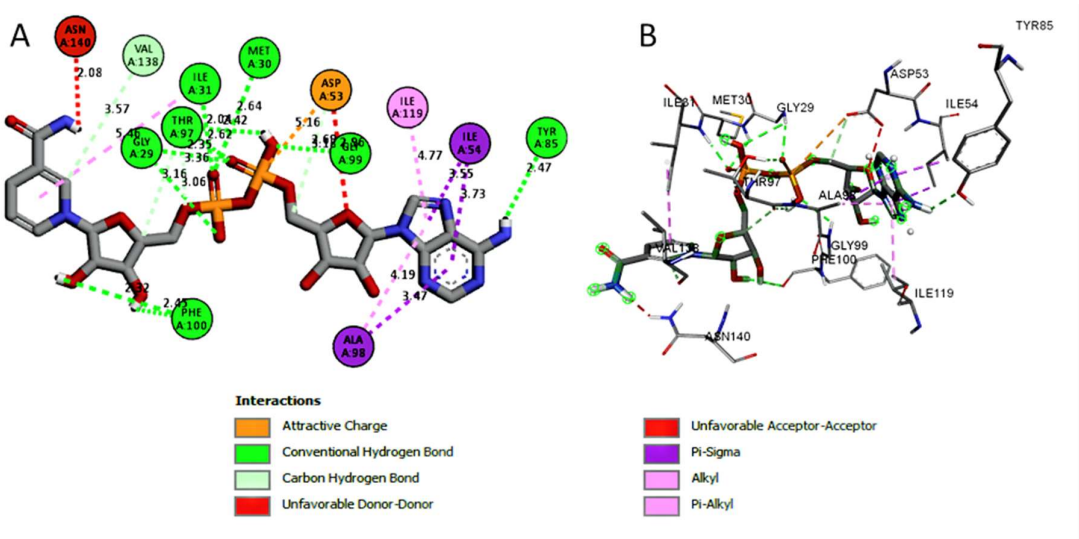

Fig. 9: A: 2D and B: 3D simulations of NADH interactions with amino acid residues at its binding site showing conventional hydrogen bonds with TYR 85, MET36, PHE100, TYR92, GLY29 and ILE31

Molecular Dynamics (MD) Simulations of Morindone-*Pf*LDH Complex

Analysis of the RMSD plot of morindone-*Pf*LDH complex MD trajectory (Fig. 5) showed that initial and instantaneous structures of the complex converged at around 10 ns with their deviations maintained largely around 3Å over the 50 ns simulation period. In the same vein, the deviations of instantaneous morindone's conformations from that of its initial conformation were maintained largely around 3Å throughout the course of the 50 ns simulation time, as decipherable from the morindone's RMSD plot (Fig. 5). Moreover, Radius of gyration (Rg) of the complex was maintained around 19.4 Å while the *Pf*LDH macromolecule itself showed significant fluctuations (about 4Å) only at two regions – residues 60 and 100 (Fig. 6).

Morindone's Interactions at the NADH Binding Site

NADH (Fig. 7), MW: 665.4 g/mol, being a huge molecule, expectedly interacted with quite a large area of *Pf*LDH's NADH

binding pocket while morindone (Fig. 7), MW: 270.24 g/mol, interacted with a relatively small area of the NADH binding site. Moreover, morindone interacted with completely different amino acid residues (Fig. 8) than the ones defining NADH interactions (Fig. 9).

DISCUSSION

Anthraquinones are redox-active natural products that are also endowed, by virtue of their planar structures, with great tendencies of macromolecular interactions [45]. In the light of the above, we conjectured anthraquinones to be possible non-competitive inhibitors of *Pf*LDH via interference with the redox function of its NADH coenzyme. In the current investigation, NADH binding site-directed multiple ligand docking was carried out on a ternary X-ray crystal model of *Pf*LDH using a library of 37 *Morinda lucida* anthraquinones as ligands. The ensuing docking results corroborated our conjecture as all of the docked compounds demonstrated considerably high binding affinities (or low binding energies), ranging from -6.6 Kcal/mol to -9.7 Kcal/mol (Table 1). However, binding affinity of ≤ 8 Kcal/mol was set for the purpose of this investigation as comparable to the -10.1 Kcal/mol binding affinity of NADH. Hence, the restriction of the subsequent *in silico* screening to top nine of the docked 37 ligands (binding affinities -8.3 Kcal/mol to -9.7 Kcal/mol) (Table 2). This evaluation was essentially pharmacokinetics-focused but epitomized as screening for drug-likeness which, in medicinal chemistry parlance, refers to the tendency or probability of a drug being orally bioavailable [46]. Drug-likeness predictions often entail the use of optimum values of a number of physicochemical parameters developed into rules or filters to select molecules with high propensity of oral bioavailability or drug-likeness at the early stages of drug discovery such that molecules that would fail later in the discovery process due to pharmacokinetic reasons could fail early [47, 48]. Such filters have different boundary values for different combinations of physical properties including molecular weight, Log P, solubility, topological surface area (TPSA), etc. [32]. They also have different levels of permitted violations based on the observations by their different authors. For instance, the Lipinski's filter which is the pioneer and most applied of all drug-likeness filters, stipulates that an orally bioavailable drug candidate must not violate more than one of four postulations of having molecular weight, Log P value, number of hydrogen bond acceptors (HBAs) and number of hydrogen bond donors (HBDs) ≤ 500 amu, 5, 10 and 5 respectively [32]. In addition to the Lipinski filter, the SwissADME webserver used for this investigation has four other drug likeness filters, namely, Gose, Verber, Egan and Muege filters, each with its characteristic boundary values of some similar physicochemical properties and permitted levels of violations [32]. A careful analysis of the drug-likeness screening results showed that while the first three of the nine hit molecules showed varying degrees of violations of both Lipinski and the other drug-likeness filters, the remaining six violated none of the stipulations of any of the five filters (Table 3).

In addition to these exclusively quantitative five rule-based filters, the SwissADME tool is equipped with a semi-quantitative rule-based oral bioavailability predictor, the Abbot's oral bioavailability score. This score, relying on total charge, TPSA and violation to the Lipinski filter, stipulates that potential orally bioavailable compounds must not have less than 10% of oral bioavailability in rats or Caco-2 cells, and groups compounds into four categories of probabilities, 11%, 17%, 56% and 85% [32]. The bioavailability scoring outcomes were consistent with those of the drug-likeness filters as the aforementioned six anthraquinones were also the ones demonstrating oral bioavailability-implying 55% bioavailability score (Table 3), meaning that each has 55% chances of achieving not less than 10% oral bioavailability in rats or Caco-2 cells.

It is noteworthy that the three anthraquinones that failed the drug-likeness screening were incidentally the ones with the best docking scores. Table 3 shows that the three of them had more than the recommended violations for each of the filters [32]. Similarly, each of them demonstrated a very low bioavailability probability score of 17%, meaning that they have 17% chances of achieving not less than 10% oral bioavailability in rats or Caco-2 cells. It is simply intellectually gratifying to note that the three of them are glycosides, more or less underscoring the negative effects that extreme polarity due to glycosylation could have on crossing biological membranes [49]. This observation underscores the roles of pharmacokinetics in drug action and why its predictions early in the drug discovery process would go a long way minimizing time, financial and trade-off losses caused by pharmacokinetic-based discovery failures. This informed dropping the three glycosylated anthraquinones, despite their high binding affinities, from the next level of screening which centered on potential toxicity prediction.

Apart from bioavailability, another key independent variable of the severe attritions that drug discovery suffers is toxicity of the drug candidate. This includes the potential to elicit minor side reactions, if the compound is endowed with capability of diverse macromolecular interactions, but, much more, on inherent ability to induce severe organ damage and cancer [50]. In this investigation, hepatotoxicity was representative of organ toxicity evaluation while cytotoxicity, carcinogenicity and mutagenicity evaluations were representative of end point toxicity evaluations useful in predicting neoplastic tendencies. While the six anthraquinones showed no hepatotoxicity, one of them 2-formyl-1-hydroxyanthraquinone (FHA) showed carcinogenic tendency (Table 4). The six of them however showed mutagenic tendencies most probably due to their flat structures which make them potential DNA double helix intercalators [51]. However, the 7000 mg/Kg LD_{50} for morindone and 5000 mg/Kg for the remaining five of them showed that whatever toxicity they are capable of eliciting would only occur at doses impracticably high for human administration. The six anthraquinones were therefore considered safe and the safest of them, morindone (LD_{50} 7000 mg/Kg), considered for molecular dynamics simulations with the possible theorizing of its binding stability under *in vivo* conditions in focus.

In vivo, every atom or molecule is in a continuous state of motion because it is found in the force fields of other atoms and/or molecules [52]. This dynamics, which can be simulated by classical mechanics using Newton's second law of motion, is unfortunately either wholly or partially ignored in docking algorithms, most of which see the macromolecule as rigid and the ligands momentarily flexible [53]. In a typical molecular dynamics simulation, pre-calculated force fields are used to initiate motion in an otherwise stationary macromolecule-ligand complex and the new coordinates of each atom monitored over a given period of simulation time that depends on the properties of interest for the study. In this investigation aimed at exploring ligand-macromolecule stability in the *in vivo* dynamic environment, a 50 ns simulation time was considered optimum for the nano-scale simulation time conventionally prescribed for such studies parameterized as root mean square deviation (RMSD), root mean square fluctuation (RMSF) and radius of gyration (Rg) [54].

RMSD is a measure of the time-based deviation from the initial rigid structure whose dynamics is being simulated. Analysis of the RMSD-time plot (fig. 5) showed a convergence of the initial and instantaneous structures of the complex at around 5 ns, maintain deviations around 3 Å throughout the 50 ns simulation time. Analysis of the RMSF plot (Fig. 6), which is a measure of the deviations of the individual residues of the protein macromolecular structure from their equilibrium positions, indicated significant fluctuations around 60th and 100th amino acid residues which incidentally were not involved in the moridone-*Pf*LDH supramolecular interactions, as could be deciphered from the latter's 2D and 3D simulations (Fig. 8) compared with those of NADH-*Pf*LDH counterparts (Fig. 9). Moreover, these isolated extreme fluctuations had little or no impact on morindone's conformation in the binding pocket as attested to by the ligand RMSD plot (Fig. 5) showing convergence as early as 2 ns and maintaining deviations below 3 Â throughout the 50 ns simulation time. These stability-implying RMSD and RMSF plots are further corroborated by the 19.4 Å radius of gyration (Rg) value (Fig. 6) for the complex [55].

CONCLUSION

This investigation has led to the identification of morindone as a potential *Pf*LDH inhibitory lead molecule. It could therefore stand as template in the development of new antimalarial agents with fast blood schizont clearance potentials, highly desirable in stemming the current rising cerebral malaria (CM) prognosis of falciparum malaria in the sub-Saharan Africa.

REFERENCES

1. Soulard V, Bosson-Vanga H, Lorthiois A, Roucher C, Franetich JF, Zanghi G, Bordessoulles M, Tefit M, Thellier M, Morosan S, Le Naour G. Plasmodium falciparum full life cycle and Plasmodium ovale liver stages in humanized mice. Nature Communications, 6(1), 2015:1-9.
2. Sato S. Plasmodium—a brief introduction to the parasites causing human malaria and their basic biology. Journal of Physiological Anthropology, 4(1), 2021:1-3.
3. Brejt JA, Golightly LM. Severe malaria: update on pathophysiology and treatment. Current Opinion in Infectious Diseases, 32(5), 2019:413-8.
4. Balaji SN, Deshmukh R, Trivedi V. Severe malaria: Biology, clinical manifestation, pathogenesis and consequences. Journal of Vector Borne Diseases, 57(1), 2020:1-13.
5. Babikir HE. Cerebral malaria in children: A review of pathophysiology, clinical manifestations and management. Journal of Paediatrics and Child Health, 10, 2010:14-23.
6. White NJ. Severe malaria. Malaria Journal, 21(1), 2022:1-17.
7. Belete TM. Recent progress in the development of new antimalarial drugs with novel targets. Drug Design, Development and Therapy, 14, 2020:3875-3889.
8. Basu S, Sahi PK. Malaria: an update. Indian Journal of Pediatrics, 84(7), 2017:521-528.
9. Hassan BM, Ahmad K, Roy S, Mohammad Ashraf J, Adil M, Haris Siddiqui, M, Khan S, Amjad KM, Provazník I. and Choi I. Computer aided drug design: success and limitations. Current Pharmaceutical Design, 22(5), 2016:572-581.
10. 10.Krungkrai J, Burat D, Kudan S, Krungkrai S, Prapunwattana P. Mitochondrial oxygen consumption in asexual and sexual blood stages of the human malarial parasite, Plasmodium falciparum. South Asian Journal of Tropical Medicine and Public Health, 30(4), 1999:636-42.
11. Ginsburg H. The biochemistry of Plasmodium falciparum: An updated overview. Advances in Malaria Research, 8, 2016:219-90.
12. Rosenthal MD, Glew RH. Medical biochemistry: Human metabolism in health and disease. John Wiley & Sons. Hoboken, U.S.A. 2009: Pp 58-101.
13. Boiteux A, Hess B. Design of glycolysis. Philosophical Transactions of the Royal Society B, 293(1063), 1981:5-22.
14. Webster KA. Evolution of the coordinate regulation of glycolytic enzyme genes by hypoxia. Journal of Experimental Biology, 206(17), 2003:2911-2922.
15. Cheung YW, Kwok J, Law AW, Watt RM, Kotaka M, Tanner JA. Structural basis for discriminatory recognition of Plasmodium lactate dehydrogenase by a DNA aptamer. Proceedings of the National Academy of Sciences, 110(40), 2013:15967-15972.
16. Deck LM, Royer RE, Chamblee BB, Hernandez VM, Malone RR, Torres JE, Hunsaker LA, Piper RC, Makler MT, Vander Jagt DL. Selective inhibitors of human lactate dehydrogenases and lactate dehydrogenase from the malarial parasite

Plasmodium falciparum. Journal of Medicinal Chemistry, 41(20), 1998:3879-3887.
17. Brady RL, Cameron A. Structure-based approaches to the development of novel anti- malarials. Current Drug Targets, 5(2), 2004:137-49.
18. Blat Y. Non-competitive inhibition by active site binders. Chemical Biology and Drug Design, 75(6), 2010:535-540.
19. Shoemark DK, Cliff MJ, Sessions RB, Clarke AR. Enzymatic properties of the lactate dehydrogenase enzyme from Plasmodium falciparum. FEBS Journal, 274(11), 2007:2738-2748.
20. Jacob C, Jamier V, Ba LA. Redox active secondary metabolites. Current Opinion in Chemical Biology, 15(1), 2011:149-155.
21. Dandawate PR, Vyas AC, Padhye SB, Singh MW, Baruah JB. Perspectives on medicinal properties of benzoquinone compounds. Mini-Reviews in Medicinal Chemistry, 10(5), 2010:436-454.
22. Diaz-Munoz G, Miranda IL, Sartori SK, de Rezende DC, Diaz MA. Anthraquinones: an overview. Studies in Natural Products Chemistry, 58, 2018 : 313-338.
23. Han YS, Heijden RV, Lefeber AWM, Erkelens C, Verpoorte R. Biosynthesis of anthraquinones in cell cultures of Cinchona 'Robusta' proceeds via the methylerythritol 4-phosphate pathway. Phytochemistry, 59, 2002:45-55.
24. Eckhard L. Biosynthesis of morindone and alizarin in intact plants and cell suspension cultures of Morinda citrifolia. Phytochemistry, 12, 1973:1669-1674.
25. Han YS, der Heiden RV, Verpoorte R. Biosynthesis of Anthraquinones in Cell Cultures of the Rubiaceae. Plant Cell, Tissue and Organ Culture, 67, 2001:201-220.
26. Dagne E, Yenesew A, Asmellash S, Demissew S, Mavi S. Anthraquinones, pre-anthraquinones and isoeleutherol in the roots of Aloe species. Phytochemistry, 35, 1994:401-406.
27. Osman CP, Ismail NH. Antiplasmodial anthraquinones from medicinal plants: the chemistry and possible mode of actions. *Natural Products Communications,* 13(12), 2018:1591-1597.
28. Karou SD, Tchacondo T, Ilboudo DP, Simpore J. Sub-Saharan Rubiaceae: a review of their traditional uses, phytochemistry and biological activities. Pakistan Journal of Biological Sciences, 14(3), 2011:149-169.
29. Pettersen EF, Goddard TD, Huang CC, Couch GS, Greenblatt DM, Meng EC, Ferrin TE. UCSF Chimera - A Visualization System for Exploratory Research and Analysis. Journal of Computational Chemistry, **25**, 2004:1605-1612.
30. BIOVIA, Dassault Systèmes, BIOVIA Workbook, 2020.
31. Dallakyan S, Olson AJ. Small-Molecule Library Screening by Docking with PyRx. In: Hempel, J., Williams, C., Hong, C. (eds) Chemical Biology. Methods in Molecular Biology, vol 1263, 2015. Humana Press, New York, NY. https://doi.org/10.1007/978-1-4939-2269-7_19
32. Daina A, Michielin O, Zoete V. SwissADME: a free web tool to evaluate pharmacokinetics, drug-likeness and medicinal chemistry friendliness of small molecules. Scientific Reports- Nature, 7, 2017: 42717. doi: 10.1038/srep42717.
33. Banerjee P, Eckert AO, Schrey AK, Preissner R. ProTox-II: a webserver for the prediction of toxicity of chemicals. Nucleic Acids Research, 46(W1), 2018: W257-W263. doi: 10.1093/nar/gky318. PMID: 29718510; PMCID: PMC6031011.
34. Abraham MJ, Murtola T, Schulz R, Páll S, Smith JC, Hess B, Lindahl E. GROMACS: High performance molecular simulations through multi-level parallelism from laptops to supercomputers. SoftwareX, 1–2, 2015: 19–25
35. Berman HM, Westbrook J, Feng Z, Gilliland G, Bhat TN, Weissig H, Shindyalov IN, Bourne PE, The Protein Data Bank. Nucleic Acids Research, 28, 2000: 235-242 https://doi.org/10.1093/nar/28.1.235.
36. Kim S, Chen J, Cheng T, Gindulyte A, He S, Li Q, Shoemaker BA, Thiessen PA, Yu B, Zaslavsky L, Zhang J, Bolton EE. Pubchem 2023 update. Nucleic Acids Research, 51 (D1), 2023: D1373-D1380. Doi: 10.1093/nar/gkac956.
37. Schüttelkopf AW, van Aalten DM. PRODRG: a tool for high-throughput crystallography of protein-ligand complexes. Acta Crystallographica Section D Biological Crystallography, 60(Pt 8), 2004:1355-63. doi: 10.1107/S0907444904011679.
38. Tian W, Chen C, Lei X, Zhao J, Liang J. CASTp 3.0: computed atlas of surface topography of proteins. Nucleic Acids Research, 46 (W1), 2018:W363-W367. doi: 10.1093/nar/gky473. PMID: 29860391; PMCID: PMC6031066.
39. The UniProt Consortium , UniProt: the Universal Protein Knowledgebase in 2023, *Nucleic Acids Research*, 51,(D1), 2023: D523–D531, https://doi.org/10.1093/nar/gkac1052
40. Dallakyan S, Olson AJ. Small-molecule library screening by docking with PyRx. Current Protocols in Chemical Biology, 2015:243-50.
41. Adewole KE, Attah AF, Adebayo JO. Morinda lucida Benth (Rubiaceae): A review of its ethnomedicine, phytochemistry and pharmacology. Journal of Ethnopharmacology. 2021 Aug 10;276:114055.
42. Mfonku NA, Tadjong AT, Kamsu GT, Kodjio N, Ren J, Mbah JA, Gatsing D, Zhan J. Isolation and characterization of antisalmonellal anthraquinones and coumarins from Morinda lucida Benth.(Rubiaceae). Chemical Papers. 2021 May;75:2067-73.
43. Rahman F, Tabrez S, Ali R, Alqahtani AS, Ahmed MZ, Rub A. Molecular docking analysis of rutin reveals

possible inhibition of SARS-CoV-2 vital proteins. Journal of traditional and complementary medicine,11(2), 2021:173-179.
44. O'Boyle NM. Towards a Universal SMILES representation-A standard method to generate canonical SMILES based on the InChI. Journal of Cheminformatics, 4, 2012:1-4.
45. Zhao H, Dietrich J. Privileged scaffolds in lead generation. Expert Opinion in Drug Discovery, 10(7), 2015:781-790.
46. Honorio KL, Moda TD, Andricopulo A. Pharmacokinetic properties and in silico ADME modeling in drug discovery. Medicinal Chemistry, 9(2), 2013:163-176.
47. Sun D, Gao W, Hu H, Zhou S. Why 90% of clinical drug development fails and how to improve it? Acta Pharmaceutical Sinica B, 12(7), 2022:3049-3062.
48. Mignani S, Rodrigues J, Tomas H, Jalal R, Singh PP. Majoral JP and Vishwakarma RA. Present drug-likeness filters in medicinal chemistry during the hit and lead optimization process: how far can they be simplified? Drug Discovery Today, 23(3), 2018:605-615.
49. Kuentz MT, Arnold Y. Influence of molecular properties on oral bioavailability of lipophilic drugs–mapping of bulkiness and different measures of polarity. Pharmaceutical Development and Technology, 14(3), 2009:312-320.
50. Roberts RA, Kavanagh SL, Mellor HR, Pollard CE, Robinson S, Platz SJ. Reducing attrition in drug development: smart loading preclinical safety assessment. Drug Discovery Today, 19(3), 2014:341-347.
51. Mukherjee A, Sasikala WD. Drug–DNA intercalation: From discovery to the molecular mechanism. Advances in Protein Chemistry and Structural Biology, 92, 2013:1-62.
52. Binder K, Horbach J, Kob W, Paul W, Varnik F. Molecular dynamics simulations. Journal of Physics: Condensed Matter, 16(5), 2004: S429.
53. Dias R, de Azevedo J, Walter F. Molecular docking algorithms. Current Drug Targets, 9(12), 2008:1040-1047.
54. Hernández-Rodríguez MC, Rosales-Hernández ME, Mendieta-Wejebe J, Martínez-Archundia M Correa-Basurto J. Current tools and methods in molecular dynamics (MD) simulations for drug design. Current Medicinal Chemistry, 23(34), 2016:3909-3924.
55. Lobanov MY, Bogatyreva NS, Galzitskaya OV. Radius of gyration as an indicator of protein structure compactness. Molecular Biology, 42, 2008:623-628.